JMB

Available online at www.sciencedirect.com

ScienceDirect

ELSEVIER

Structural Mechanism of Transcriptional Autorepression of the *Escherichia coli* RelB/RelE Antitoxin/Toxin Module

Guang-Yao Li[1], Yonglong Zhang[2], Masayori Inouye[2] and Mitsuhiko Ikura[1]*

[1]*Division of Signaling Biology, Ontario Cancer Institute and Department of Medical Biophysics, University of Toronto, Toronto, Ontario, Canada M5G 1L7*

[2]*Department of Biochemistry, Robert Wood Johnson Medical School, University of Medicine and Dentistry of New Jersey, Piscataway, NJ 08854, USA*

Edited by M. F. Summers

The *Escherichia coli* chromosomal *relBE* operon encodes a toxin–antitoxin system, which is autoregulated by its protein products, RelB and RelE. RelB acts as a transcriptional repressor and RelE functions as a cofactor to enhance the repressor activity of RelB. Here, we present the NMR-derived structure of a RelB dimer and show that a RelB dimer recognizes a hexad repeat in the palindromic operator region through a ribbon–helix–helix motif. Our biochemical data show that two weakly associated RelB dimers bind to the adjacent repeats in the 3'-site of the operator (O_R) at a moderate affinity (K_d, $\sim 10^{-5}$ M). However, in the presence of RelE, a RelB tetramer binds two distinct binding sites within the operator region, each with an enhanced affinity (K_d, $\sim 10^{-6}$ M for the low-affinity site, O_L, and 10^{-8} M for the high-affinity site, O_R). We propose that the enhanced affinity for the operator element is mediated by a cooperative DNA binding by a pair of RelB dimers and that the interaction between RelB dimers is strongly augmented by the presence of the cognate toxin RelE.

Introduction

Bacterial toxin–antitoxin (TA) systems generally consist of a toxin protein and a cognate antitoxin protein.[1–3] Two open reading frames encoding a toxin gene and an antitoxin gene are always found in pairs within the same TA operon.[4] Because the antitoxin is susceptible to proteolysis, new protein synthesis is constantly required to maintain a steady-state level of antitoxin, which forms an inhibitory complex with the toxin. Consequently, protein synthesis is negatively autoregulated by a feedback mechanism, in which the antitoxin acts as a transcriptional repressor and the toxin acts as a corepressor. TA systems are found in both plasmids and chromosomes. In daughter cells that fail to inherit the TA genetic elements, proteolysis of the antitoxin in the absence of new supplied antitoxin results in the release of the long-lived toxin that exerts its deleterious effect upon the host organism. The plasmid-borne TA systems affect the inheritance of their host plasmids by postsegregational killing of cells that become plasmid free. The cells become "addictive" to the plasmid hosting TA systems.[5] The chromosomal TA systems were generally proposed to act as metabolic stress response elements.[3,6] For instance, the *relBE* system plays a role in the cellular response to amino acid deprivation.[7] Upon entering nutritional starvation condition, transcription from the *relBE* operon is increased dramatically, while the level of RelB antitoxin is reduced as a result of Lon-dependent proteolysis. Consequently, RelE toxin is liberated, leading to cell growth arrest or eventually cell death.[8]

*Corresponding author. E-mail address: mikura@uhnres.utoronto.ca.

Abbreviations used: TA, toxin–antitoxin; RHH, ribbon–helix–helix; HSQC, heteronuclear single quantum coherence; CSI, chemical shift index; NOE, nuclear Overhauser enhancement; SEC, size-exclusion chromatography; MALS, multiple-angle light scattering; CCL, chemical cross-linking; dsDNA, double-stranded DNA; NOESY, nuclear Overhauser enhancement spectroscopy; EMSA, electrophoretic mobility shift assay; PDB, Protein Data Bank.

The *Escherichia coli* RelBE system is one of the most extensively investigated TA systems. *In vitro* studies have documented that association of RelE at the ribosome A site promotes a novel ribonucleolytic activity that cleaves mRNA codons, preferentially between the second and the third nucleotides of the termination codons.[8,9] This activity leads to global inhibition of protein synthesis. Homologs of the RelBE system have been found in different kinds of bacteria and archaeon in both chromosomes and plasmids and shown to be functionally active.[3,10,11]

A crystal structure of $RelB_2$–$RelE_2$ from the hyperthermophilic archaeon *Pyrococcus horikoshii* ($aRelB_2$–$aRelE_2$) has been solved recently.[12] In the tetrameric complex, a molecule of aRelB wraps around a compact aRelE, forming a tight heterodimer. Two such heterodimers are tethered together by two noncontact aRelB through the interactions between aRelB from one heterodimer and aRelE from another (Fig. S1b). Despite this elegant structural study on the TA recognition of this TA system, it is still unclear how RelB alone and the RelB–RelE complex regulate transcription of the *relBE* gene via direct binding to the promoter region. The sequence similarity between the archaeal *P. horikoshii* aRelB and bacterial *E. coli* RelB is relatively low, with 24% identity and 48% similarity (Fig. S1a). High level of homology only resides within the C-terminal part of these antitoxins. The sequence variation in the N-terminus indicates that *E. coli* RelB may employ a different method for the transcriptional regulation.

In the present article, we employed biochemical and structural techniques to characterize *E. coli* RelB, the RelB–RelE complex, and their interactions with the promoter DNA, in order to explore the transcriptional regulation mechanism of the *E. coli relBE* system. In contrast to the previous notion that free RelB is unstructured,[12,13] our present study shows that RelB forms a tetramer with extensive secondary structure in solution and interacts with a hexad repeat sequence (5′-TTGTAA-3′) in the promoter region with moderate affinity (10^{-5} M). High affinity
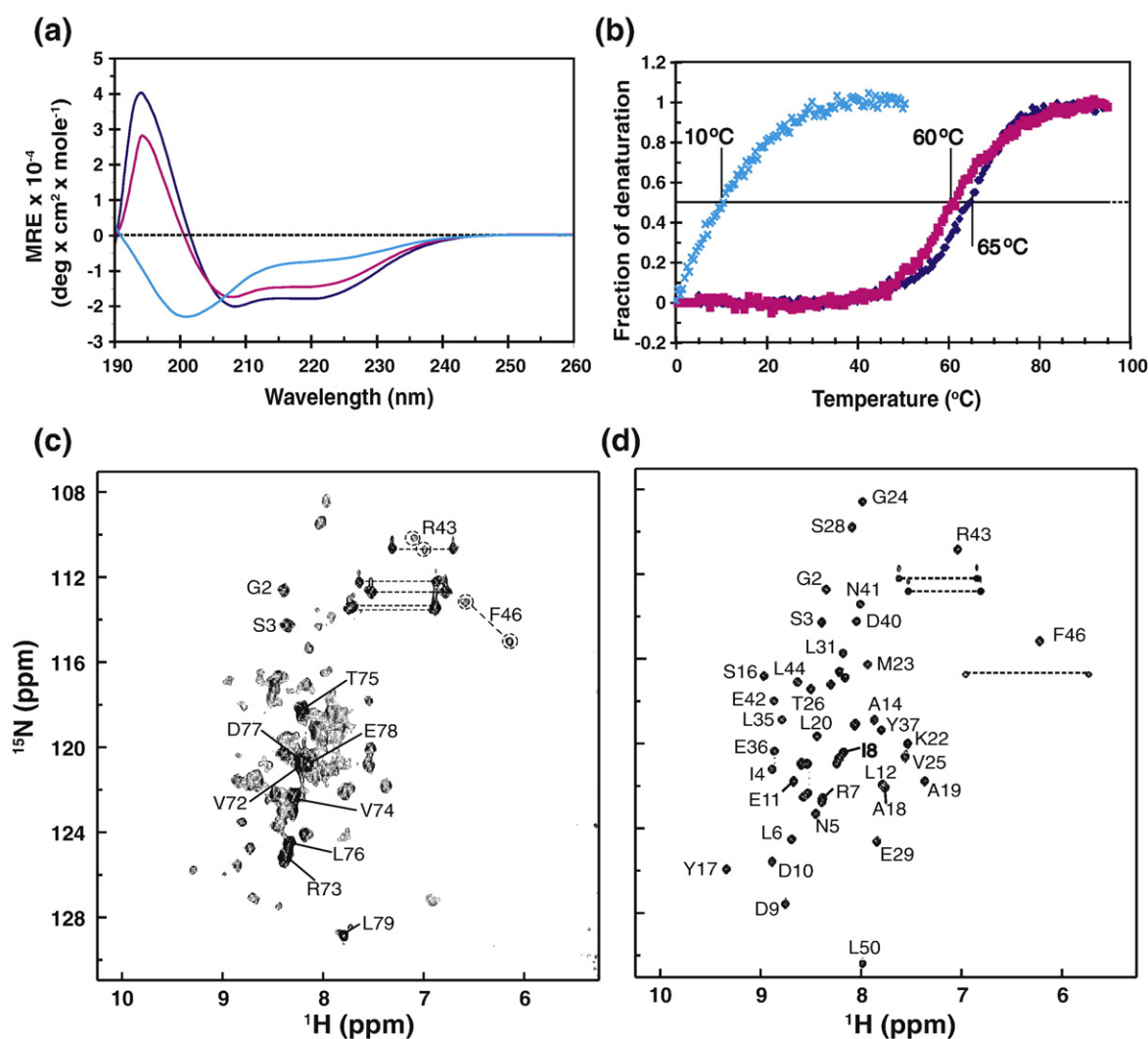

Fig. 1. Characterization of *E. coli* RelB by CD and NMR spectroscopy. Far-UV CD spectra (a) and thermal denaturation curves (b) of the full-length RelB (1–79, magenta), $RelB_N$ (1–50, dark blue), and $RelB_C$ (47–79, cyan) were recorded in 20 mM NaPi and 50 mM NaCl, pH 7.0. The ^1H–^{15}N HSQC spectra of the full-length RelB (c) and $RelB_N$ (d) were measured in 20 mM NaPi, 100 mM NaCl, and 1 mM DTT, pH 6.5, at 30 °C.

for DNA (10^{-8} M) is only achieved in the presence of RelE. Elucidation of the structure of the RelB DNA binding domain by nuclear magnetic resonance (NMR) spectroscopy revealed that RelB is a member of the ribbon–helix–helix (RHH) family of transcription factors as predicted based on sequence[11,14] (Fig. S1). Our quantitative analysis on the synergistic interactions within the RelBE module and the promoter DNA provides a basis for understanding this genetic and biochemical regulatory circuitry.

Results

Characterization of RelB domains

The *E. coli* RelB antitoxin is a small acidic protein composed of 79 amino acids (Fig. S1) with a theoretical isoelectric point of 4.95, in contrast to most of the DNA binding proteins, which are more basic. The circular dichroism (CD) spectrum of recombinant RelB exhibits distinct minima at 208 and 222 nm, characteristic of the presence of α-helical structure (Fig. 1a). Deconvolution of the CD spectrum with the CDSSTR software[15] demonstrates that RelB contains 53% α-helices, 10% β-strands, and 37% turns and random coils, which is consistent with the secondary structure prediction by the PSIPRED software[16] (Fig. S1a). RelB melts in a cooperative and reversible manner with a T_m at 60 °C, which confirms that RelB is a folded protein with relatively high heat stability (Fig. 1b). However, the ^{1}H–^{15}N heteronuclear single quantum coherence (HSQC) spectrum of a ^{15}N-labeled RelB sample suffered from severe line-width broadening for the majority of cross peaks, suggesting that RelB may associate into oligomers in solution (Fig. 1c). A few sharp resonances among these broadened peaks were assigned as residues from the C-terminus (Val72–Leu79). These residues clearly represent the flexible parts of the molecule with high mobility. The spectrum also contained a number of doublet peaks for residues from various regions including loop α2–α3 (i.e., R43, F46, etc.). While it is unclear at present what is the origin of the peak doubling, we suggest that the molecule may be asymmetric when RelB is in an isolated oligomer or that RelB is present in different conformations in solution (Fig. 1c).

In order to optimize RelB for further structural studies, we designed several constructs with various C-terminal deletions (Table 1). Firstly, the protein was truncated after Lys70 in order to remove the last nine residues, which appeared to be highly flexible from the previous NMR result (Fig. 1c). The RelB$_{1–70}$ construct exhibited a spectrum in which the sharp peaks originating from the C-terminal residues were absent; however, it was otherwise similar to the wild type, with broadened resonances and the doublet peaks (Fig. S2a). These observations indicate that RelB$_{1–70}$ retains the same tertiary or quaternary structure as the full-length RelB. Limited trypsin

Table 1. Oligomerization of RelB constructs and the RelB–RelE complex

	Calc. mass[a] (kDa)	SEC (kDa)	MALS (kDa)	CCL (kDa)	Oligomeric states
RelB$_{1–79}$	9.35	66.9	38.1 ± 1.5	∼40	Tetramer
RelB$_{1–70}$	8.33	50.6	32.8 ± 2.6	∼33	Tetramer
RelB$_{1–65}$	7.72	33.7	16.3 ± 1.1	∼16	Dimer
RelB$_{1–50}$	5.99	15.7	12.2 ± 0.7	n.d.	Dimer
RelB–RelE[b]	9.1; 12.2	48.7	42.4 ± 3.8	n.d.	Tetramer

n.d., not detected.
[a] The molecular mass of each protein was calculated, including the residual fusion tag from the expression vector.
[b] A nontagged RelB–RelE complex (described in Methods and Experiments) showed the same stoichiometry and compact conformation as this His-tagged one, indicating that the His tag at the C-terminus of RelE has little impact on the complex assembly.

digestion was then carried out on the full-length RelB in order to identify stable folded domains. A trypsin-resistant fragment of 7.8 kDa was identified as Met1–Arg65 by mass spectroscopy (Fig. S2b). A construct corresponding to this fragment (RelB$_{1–65}$) produced well-dispersed NMR spectra (Fig. S2c), enabling us to assign most of the backbone ^{1}H, ^{13}C, and ^{15}N nuclei through standard triple-resonance experiments.[17,18] A chemical shift index (CSI) analysis[19] revealed that a strand–helix–helix structural motif exists in the N-terminal region from Met1 to Glu42. The following part (Arg43 to Arg65) is largely unstructured as evidenced by random CSI values and low heteronuclei (^{1}H–^{15}N) nuclear Overhauser enhancement (NOE) values (Fig. S2d and e). Based on these analyses, we divided the full-length RelB into two separated domains for further structural studies: an N-terminal domain, Met1–Leu50 (RelB$_N$), and a C-terminal domain, Lys47–Leu79 (RelB$_C$).

The CD spectrum of RelB$_N$ shows characteristics of a well-folded protein domain (60% alpha and 13% beta), and its thermal stability (T_m) increases by 5 °C compared with the full-length RelB (Fig. 1a and b). The heat denaturation process of RelB$_N$ is completely reversible as seen in the full-length RelB. In contrast to RelB$_N$, the CD spectrum of RelB$_C$ recorded at 20 °C is characteristic of random coil (Fig. 1a). However, at lower temperatures, CD spectra start to show indications of helical structure, as evidenced by a temperature-dependent decrease in ellipticity at 222 nm. The apparent melting temperature of RelB$_C$ was estimated to be below 10 °C (Fig. 1b). In summary, antitoxin RelB possesses a well-folded core domain (Met1–Glu42) at its N-terminus followed by a flexible region (Arg43–Leu79) at its C-terminus, a modular pattern typical of many other antitoxins.[20–22]

Oligomerization of RelB

In order to evaluate the oligomeric state and the global compactness of RelB, we employed several biophysical methods, including size-exclusion chromatography (SEC), multiple-angle light scattering (MALS), and chemical cross-linking (CCL) on four

constructs: $RelB_{1-50}$, $RelB_{1-65}$, $RelB_{1-70}$, and full-length $RelB_{1-79}$. Firstly, size-exclusion analysis of RelB (9.38 kDa) yielded an apparent molecular mass (66.9 kDa) that is significantly larger than that of a dimer (as exhibited by many other antitoxin dimers) and closer to that of a septamer. Since the determination of molecular mass by SEC is related to the shape of the molecule, it is less accurate with non-globular proteins. It is likely that the SEC method overestimates the size of RelB because the unstructured C-terminal region does not fold into a compact globular conformation. The molecular weights of $RelB_{1-65}$ and $RelB_{1-70}$ were similarly overestimated by the SEC method (Table 1).

To more accurately evaluate the stoichiometries of RelB and its deletion mutants, we employed the methods of MALS (Fig. S3 and Table 1) and CCL (Fig. S4 and Table 1), which are less dependent of molecular shape. Since the molecular weight determined by SEC will more closely match that determined by MALS when a protein is compact and globular, we determined that $RelB_N$ (M_{SEC}/M_{MALS}, 1.2) is more compactly folded compared with the other constructs (M_{SEC}/M_{MALS}: $RelB_{1-70}$, 1.5; $RelB_{1-79}$, 1.8; $RelB_{1-65}$, 2.1). $RelB_{1-65}$ shows the least compactness probably because the truncation breaks down the formation of the putative helix α3 (Fig. S1). CCL data are in agreement with the MALS-derived molecular size estimation (Table 1). Taken together, the full-length RelB and $RelB_{1-70}$ are tetrameric while $RelB_{1-65}$ and $RelB_N$ are dimeric in solution. These results strongly argue that the core domain forms a stable dimeric structure and that the C-terminal region is responsible for dimerization of the dimeric core domain, which results in the assembly of RelB tetramer.

Subsequently, we applied the same analysis on the copurified RelB–RelE complex with a His tag at the C-terminus of RelE. The RelB–RelE complex (RelB, 9.1 kDa; $RelE_{c-his}$, 12.2 kDa) eluted as a single peak with an apparent molecular mass of 48.7 kDa from SEC and 42.4 kDa from MALS, both of which fit well with a stoichiometry of $RelB_2$–$RelE_2$ heterotetramer (42.6 kDa). The consistency between SEC and MALS measurements (M_{SEC}/M_{MALS}, 1.15) indicates that the complex of RelB and RelE forms a relatively globular fold, as opposed to the nonglobular shape of free RelB. A disorder-to-order transition may be induced in the C-terminal region of RelB upon RelE binding.[14]

Mapping the operator sequence in *relBE* promoter

It has been reported that antitoxin RelB is responsible for the transcriptional regulation of the *relBE* gene by an autorepression mechanism that is enhanced by toxin RelE.[23,24] This transcriptional repression function appears to be mediated by binding of the repressor protein at a palindromic sequence in a length of 24 bp (Fig. 2a). This region contains three pseudo-palindromic DNA hexad repeats (direct 5′-TTGTAA-3′ or invert 5′-TTA-

CAA-3′) and a similar hexad (5′-TgACAt-3′) with four out of six bases matching the consensus hexad sequence. These four repeats cover the region between the −10 box and the ribosome binding site, indicating that they might be the potential binding site for the transcription factor RelB.

We employed an *in vitro* transcription assay in the presence of RelB and the RelB–RelE complex to identify their *bona fide* operator sites within the promoter region. In the assay, RelB represses the transcription of its own gene *in vitro*, and the addition of RelE significantly enhanced the repression of transcription by RelB (Fig. 2b). Gel shift assays were employed using a 150-bp DNA fragment encompassing the promoter region of the *relBE* gene to determine the stoichiometry of these complexes. Both RelB alone and the RelB–RelE complex retard the mobility of the DNA fragment in a concentration-dependent mode, indicating a specific protein–DNA interaction (Fig. 2c). However, the patterns of gel shifts are different. In the presence of the RelB–RelE complex, a well-defined single shifted band is detected regardless of the concentration of the RelB–RelE complex. In contrast, RelB alone induced a defined but faint band at its low concentrations and gradually shifted into much higher molecular weight bands as the RelB concentration increases (Fig. 2c). These higher molecular weight bands are likely attributed to the oligomerization or aggregation of RelB, which assembles on the surface of the promoter DNA (see Discussion). These observations lead to speculation that multiple subsites may exis in the promoter region of the *relBE* gene, each with different affinities for RelB, as described for many other TA systems including *ccdAB*,[21,25] *parDE*,[22] and ω/ε/ζ.[26] Alternatively, RelE may stabilize the conformation of RelB and prevent its further oligomerization on the surface of DNA.

A DNase I footprinting assay was carried out in order to delineate the consensus sequence elements for RelB binding. In this assay, a 12-bp sequence composed of two adjacent palindromic hexad repeats located in the downstream of the 24-bp putative operator region was significantly protected by either RelB alone or the RelB–RelE complex (Fig. 2d). This result indicates that RelB and the RelB–RelE complex may have higher affinity with the downstream (right, O_R) side of the operator compared to the upstream (left, O_L) side (Fig. 2a).

In order to characterize the organization and cooperative properties of the binding sites within the promoter region, we further dissected the operator repeats region into three different lengths of double-stranded DNA (dsDNA) oligonucleotides: dsDNA-I, -II, and -III (Table S1). Surface plasmon resonance (SPR) analysis was employed to compare the interactions of RelB constructs (RelB, $RelB_N$, $RelB_{R7A}$, and RelB–RelE) with these DNA duplexes, which were tagged with biotin and immobilized on a streptavidin chip. RelB and $RelB_N$ produced similar sensorgram profiles with steep association and dissociation curves when flowed over any of the chip channels captured, dsDNA-I, -II, or -III (Fig.
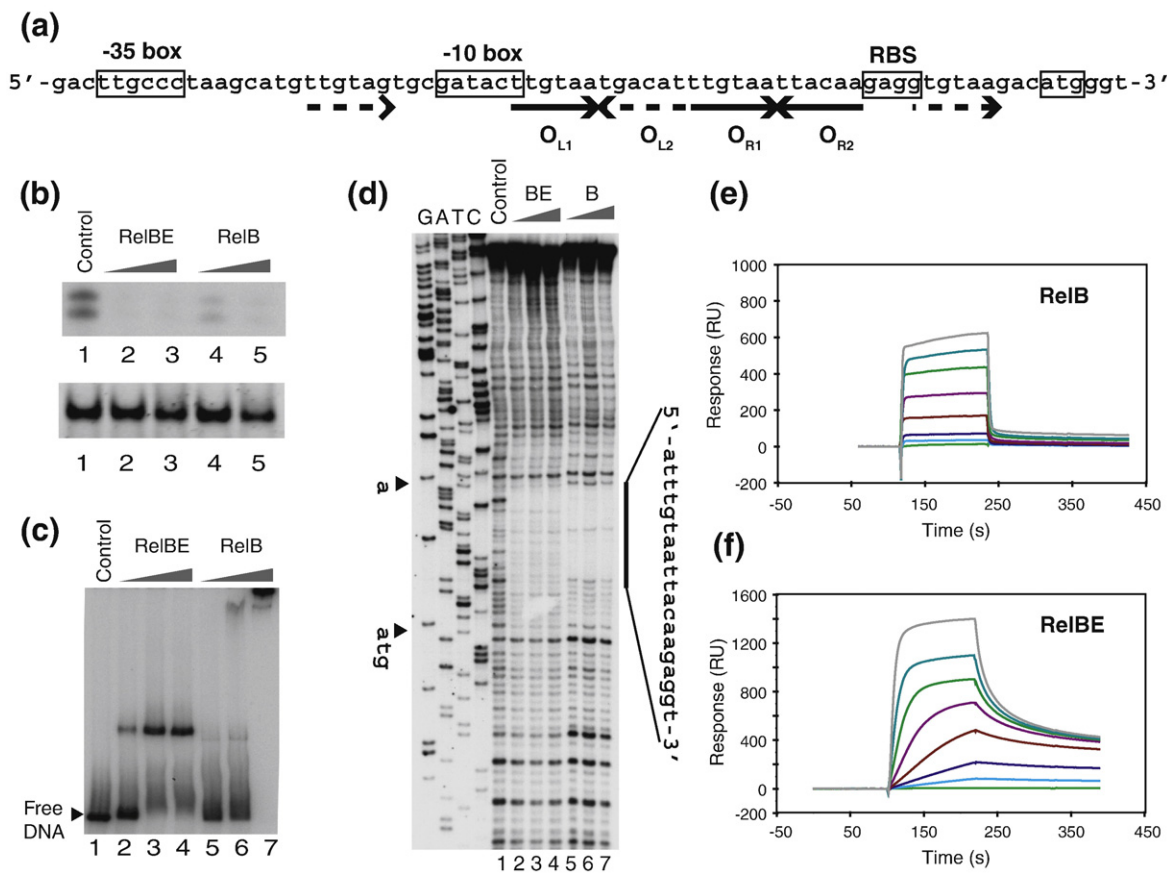
Fig. 2. The organization of operator sites in the *relBE* promoter region. (a) The operator sequence upstream of the *relBE* gene. The −35 site, −10 site, ribosome binding site (RBS), and the translation start codon of *relB* are indicated with boxes. Solid or broken arrows denote the hexad repeats recognized by RelB. (b) *In vitro* transcription assay in the presence of the RelB–RelE complex and RelB. The upper panel shows the transcribed RNA fragments using the *relBE* template gene, and the lower panel shows the control assay on the *mazG* mRNA fragment. In both panels: lane 1, no protein; lanes 2 to 3, the RelB–RelE complex (1, 5 μg); lanes 4 to 5, RelB (1, 5 μg) were added. (c) An EMSA on the 150-bp *relBE* promoter region. Lane 1, no protein; lanes 2 to 4, the RelB–RelE complex (1, 5, and 50 μg); lanes 5 to 7, RelB (1, 5, and 50 μg) were added. (d) DNase I footprinting of the *relBE* promoter region. Lane 1, no protein; lanes 2 to 4, the RelB–RelE complex (1, 5, and 50 μg); lanes 5 to 7, RelB (1, 5, and 50 μg) were added. The transcription and translation initiation sites are labeled with 'a' and 'ATG' at the left side. The protected palindromic sequences are outlined at the right side. (e) SPR assay of the interaction between dsDNA-III and RelB (0, 1, 3, 10, 25, 50, 75, and 100 μM). (f) SPR assay of the interaction between dsDNA-III and the RelB–RelE complex (0, 0.0156, 0.0312, 0.0625, 0.125, 0.25, 0.5, and 1.0 μM).

2e). The apparent dissociation constants (K_d), calculated via a steady-state affinity model, indicate that $RelB_N$ binds to these three DNA oligomers with affinities in the range of 200–300 μM (Table 2). The relative maximum responses, which are related to the mass of the proteins captured on the surfaces,

were proportional to the number of hexad repeats present in the immobilized DNA. These observations indicate that one hexad repeat represents a primary binding site for one dimeric DNA binding domain of RelB. Hence, $RelB_N$ binds to the four binding sites within the operator region with a similar affinity and shows no evidence for cooperative binding when the sites are linked.

The full-length RelB binds to the single-site DNA oligomers (dsDNA-I) weakly with a similar affinity to $RelB_N$. However, the DNA binding affinities of RelB to dsDNA-II or -III, which contain two or four sites, respectively, increase significantly by 10- to 20-fold, whereas $RelB_N$ does not (Table 2). These results strongly suggest that the tetramerization of RelB via the C-terminal portion is required for the enhanced affinity on recognition of multiple DNA elements. Our SPR experiments also demonstrate that the presence of RelE dramatically enhanced the affinity of RelB to dsDNA-II or -III (but not dsDNA-I),

Table 2. DNA binding affinities of RelB constructs and the RelB–RelE complex

Protein	dsDNA-I (12 bp)	dsDNA-II (20 bp)	dsDNA-III (32 bp)
$RelB_{1-50}$	2.84×10^{-4} M	2.10×10^{-4} M	1.97×10^{-4} M
$RelB_{1-79}$	2.60×10^{-4} M	2.12×10^{-5} M	1.25×10^{-5} M
RelB–RelE	n.d.	7.14×10^{-8} M	1.86×10^{-6} M
			2.34×10^{-8} M
$RelB_{R7A}$	n.d.	n.d.	n.d.

The concentration of proteins was calculated according to the oligomeric state as characterized in Table 1. n.d., not detectable.

indicating that stabilization of the RelB tetramer by RelE markedly improves the DNA binding affinity (Table 2 and Fig. 2f). The binding of the RelB–RelE complex to dsDNA-II is best described by a Langmuir 1:1 binding model, although there are two potential binding sites for a RelB–RelE complex. The apparent K_d derived from the global fitting is 7.14×10^{-8} M. This may indicate that the two sites in dsDNA-II are highly coupled or have similar affinities, which could not be measured separately. In the case of dsDNA-III, which has four binding sites, the binding curves are well fitted globally to a sequential binding model. The fitting result shows two apparent K_d values of 1.86×10^{-6} M and 2.34×10^{-8} M, respectively. Together with the result of the footprinting assay (Fig. 2d) and an inspection of the sequence of hexad repeats within dsDNA-III (Fig. 2a), the existence of two different affinities suggests that the higher affinity site is the perfect palindrome in the right side (downstream) of the operator, O_R, and the lower affinity site is the left side imperfect palindrome, O_L. These data demonstrate that synergetic binding is induced not only between the two subsites (O_{R1}, O_{R2}) within O_R but also between O_R and O_L, within the entire promoter region, which enhances the affinity of O_R by three times in dsDNA-III compared with dsDNA-II. The DNA binding activity of the full-length RelB is completely abolished by the single mutation R7A (Table 2), suggesting that this positively charged arginine residue is critical for DNA recognition.

Structure of the DNA binding domain of RelB

The number of amide resonances observed in the ^1H–^{15}N HSQC spectrum corresponds to the number of residues in each monomer, demonstrating that the RelB$_N$ dimer is symmetrical (Fig. 1e). The high quality of three-dimensional (3D) heteronuclear correlation and NOE spectroscopy (NOESY) experiments allowed for approximately 97% complete proton chemical shift assignments. Intersubunit constraints were obtained from a $^{13}C/^{15}N$-filtered/edited 3D NOESY experiment.[27] The structure of RelB$_N$ was calculated using CYANA,[28] with the knowledge that the structure would be a symmetric dimer. The 20 lowest energy structures were refined in water as the explicit solvent and validated with ^1H–^{15}N residual dipolar coupling constraints using CNS.[29] The input constraints and the structure statistics of RelB$_N$ conformers are summarized in Table 3.

The overall structure of RelB$_N$ consists of two tightly intertwined subunits, combined to form a single hydrophobic core (Fig. 3). Each subunit comprises a β-strand, β1 (residues 3–7), followed by two α-helices, α1 and α2 (residues 12–23 and 28–40), connected by short loop regions (Fig. 3a). The β-strands from each subunit assemble to form an antiparallel β-sheet with four α-helices packed together beside this β-structure. Numerous branched hydrophobic residues from both monomers form a compact hydrophobic core, specifically from β-strands (Ile4, Leu6, and Ile8), α1 (Leu12 and

Table 3. NMR structure statistics

	Value
NMR distance and dihedral constraints	
Total NOE distance limits	2994
Intraresidue	708
Sequential: $|i-j|=1$	820
Medium range: $1<|i-j|<5$	754
Long-range: $|i-j|\geq 5$	712
Intermolecular	577
Hydrogen bonds[a]	52×2
Dihedral angle restraints	
ϕ	68
ψ	68
RDC restraints (HN)	84
Structure statistics[b]	
Violations (mean±SD)	
Number of distance violations: >0.3 Å	0.875±0.222
Number of dihedral violations: >5°	0.976±0.499
Maximum distance constraint violation (Å)	0.475
Maximum dihedral angle violation (°)	7.180
Distance constraint r.m.s.d. (Å)	0.013±0.001
Dihedral angle constraint r.m.s.d. (°)	0.117±0.055
Idealized geometry deviations (mean±SD)	
Bond lengths (Å)	0.007±0.000
Bond angles (°)	0.755±0.016
Impropers (°)	1.442±0.121
Ramachandran statistics (% of residues)[c]	
Most favored regions	89.6
Additional allowed regions	6.9
Generously allowed regions	0.8
Disallowed regions	2.7
Average pairwise r.m.s.d. (Å)[d]	
Heavy (to mean)	0.93±0.14
Backbone (to mean)	0.35±0.08

r.m.s.d., root-mean-square deviation; SD, standard deviation; RDC, residual dipolar coupling.
[a] Based on C^α–C^β chemical shift indices and amide exchange data.
[b] Mean and SD calculated from the 20 lowest energy dimeric structure ensemble.
[c] Calculated for 20 dimer ensemble using PROCHECK–NMR.
[d] Calculated for ensemble using MOLMOL.

Leu20), and α2 (Leu31, Met34, Leu35, and Ile38) (Fig. 3b and c). The side chains of these residues from both subunits are directed toward the interior of the protein, forming a tightly packed core as well as the dimeric interface. This type of intermolecular antiparallel β-sheet and the tightly packed hydrophobic intersubunit interface are typical in the structure of dimeric RHH proteins.[30–32]

The RelB$_N$ structure indicates that *E. coli* RelB belongs to the RHH family of prokaryotic transcription factors, which is consistent with the sequence-based prediction[11,14] (Fig. S1). However, it differs to its archaeal orthologue from *P. horikoshii*. In the aRelB$_2$–aRelE$_2$ complex, aRelB is mainly composed of two parallel helices separated by a long loop (Fig. S1b). Interestingly, the symmetry-related helices α1 can form a four-helix bundle around a crystallographic 2-fold axis (Fig. S1c). Based on these observations, aRelB was hypothesized to recognize DNA as a dimer via a leucine zipper motif.[12,33] The present structure of RelB$_N$ clearly demonstrates that *E. coli* RelB uses a mechanism different from that proposed for the archaeal aRelB.
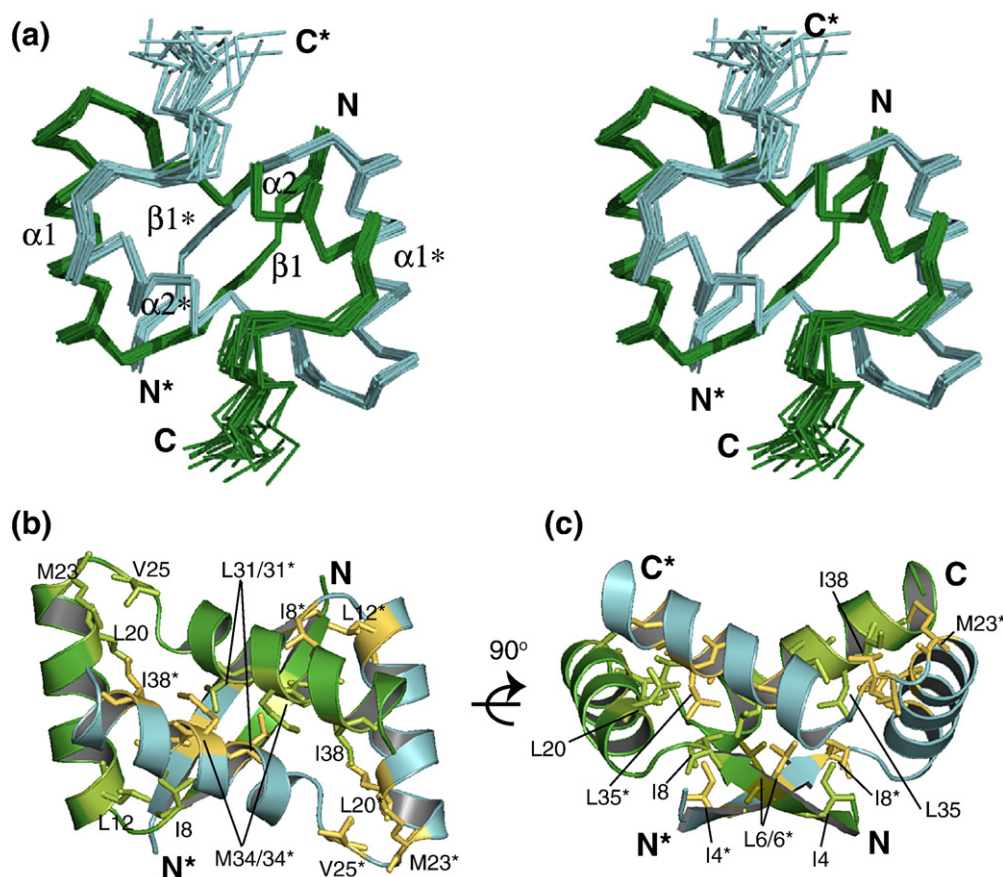
Fig. 3. Structure of RelB$_N$ determined by NMR spectroscopy. (a) Stereoview of the backbone ensemble of the 20 lowest energy structures of RelB$_N$. The two subunits are colored green and cyan. (b) Ribbon representation of the lowest energy structure of RelB$_N$. Residues involved in the formation of the hydrophobic interface from both subunits are represented as sticks and labeled with residue name and number (residues with or without * represent from different subunit). (c) is the view of 90° rotation of (b) along the *x*-axis.

Characterization of the interaction between RelB and DNA by NMR

NMR titration experiments on RelB$_N$ with two DNA fragments, dsDNA-I and -II, were carried out to map specific residues involved in DNA binding. Addition of DNA fragments to a ^{15}N-labeled sample of RelB$_N$ resulted in chemical shift changes for a number of cross peaks in a fast-exchange regime on the NMR time scale (Fig. 4a and b). As RelB was titrated with DNA, the signal intensities of the amide groups of Leu6, Arg7, and the side-chain H$_\delta$ protons of Asn5 gradually diminished, strongly suggesting that these residues make direct contact with the DNA and that the peaks are broadened due to exchange between free and bound states with large chemical shift differences (Fig. 4b). In addition to these broadened residues, Gly2, Ser3, and Ile8 exhibited significant chemical shift perturbation. These broadened and perturbed residues (2–8) are located within the intersubunit β-sheet of the RelB$_N$ dimer, and these data suggest that this region forms the primary contact with the DNA operator. Another cluster of residues (including Ser28–Leu31) that were perturbed upon DNA binding are situated in the N-terminus of the helix α2 (Fig. 4c). These two clusters of residues are highly conserved among RHH domains and are known to bind to the DNA operator site.[32] Several hydrophobic residues from the dimerization interface (L33, L35, and Y37) exhibit chemical shift changes but are not directly involved in DNA binding. The rate of monomer-to-dimer exchange may be impacted by the presence of DNA, consequently altering the chemical environment or dynamic behavior of these residues. In contrast, the loop regions and the C-terminus of RelB$_N$ are least perturbed in the NMR spectra.

A comparison of the residues exhibiting chemical shift perturbation (Fig. 4d) and the distribution of positive electrostatic charge (Fig. 4e) on the contact surface of RelB$_N$ clearly demonstrates that electrostatic effects play an important role in orienting RelB onto the surface of DNA. The DNA binding surface on RelB$_N$ displays an overall positive electrostatic potential around the β-sheet and flanking residues Arg7 and Lys13. There is also a highly negative electrostatic potential on the periphery of the positive binding surface near the loop residues Asp9, Asp10, and Glu11. These residues have the least chemical shift perturbation, indicating that they are not directly involved in the contact with DNA. It is possible that the negative charge plays a role in
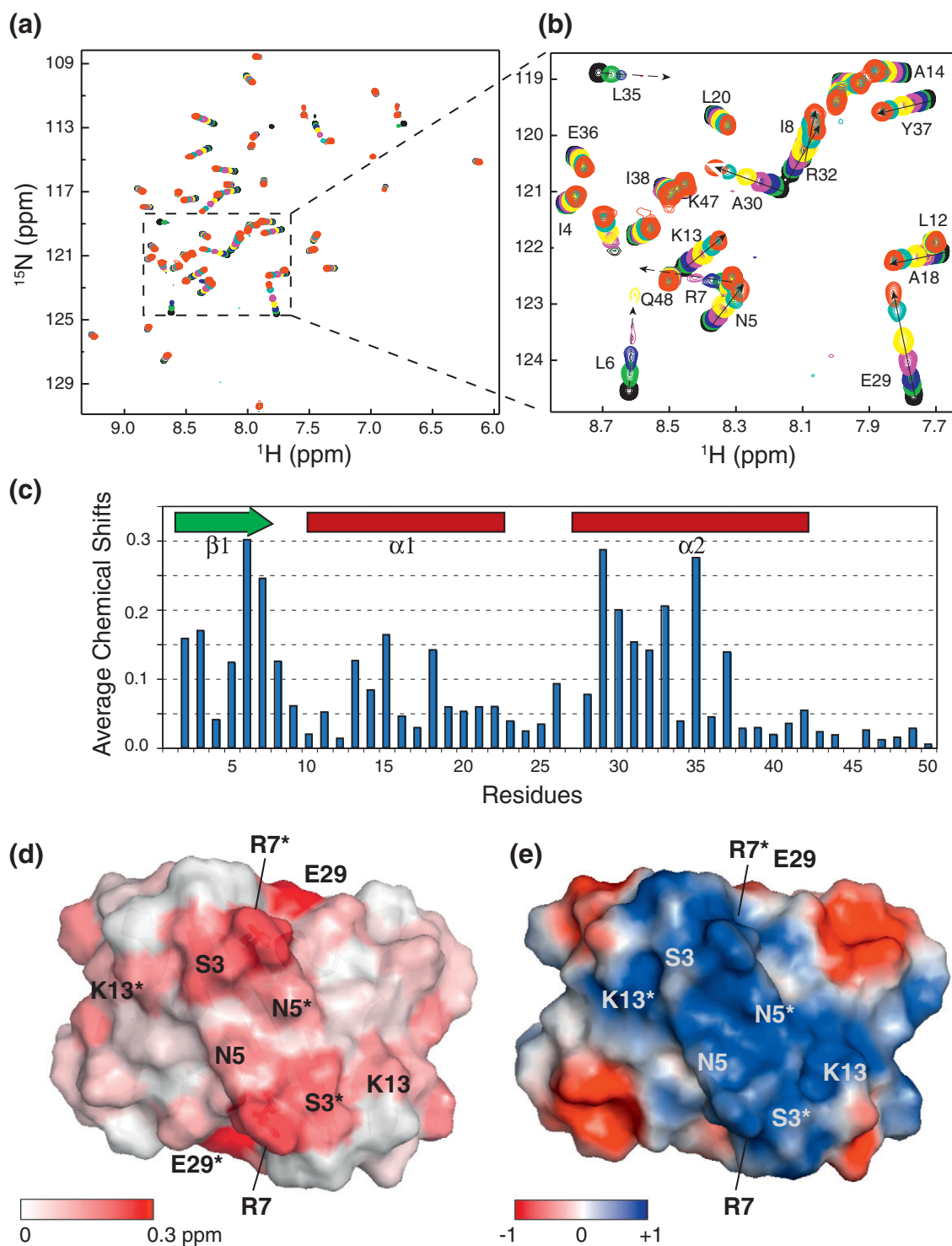
Fig. 4. DNA titration and chemical shift mapping of the DNA binding surface. (a and b) Superposition of ^1H–^{15}N HSQC spectra of RelB$_N$ titrated with dsDNA-II at a ratio of [dsDNA]/[RelB$_{N2}$] from 0 to 2. The residues with significant chemical shift changes are labeled with arrows and residues. (c) The average chemical shift changes are plotted against residues with secondary structure elements indicated. (d) The surface model of RelB$_N$ colored by chemical shift perturbations. (e) Electrostatic surface of RelB$_N$ calculated by APBS[34] and plotted by PyMOL.[35]

directing the major groove onto the adjacent positively charged surface of RelB by repelling the phosphate backbone.

A homology model of the RelB–DNA complex based on the crystal structures of Arc-DNA[36] and ω-DNA[26] shows that, upon binding of RelB$_N$ to DNA,

the β-sheet inserts into the DNA major groove (Fig. 5a and b). Three hydrophilic amino acid side chains (Ser3, Asn5, and Lys7) from each strand point into the groove and make crucial sequence-specific nucleotide base contacts. The N-terminus of the second α-helix α2 is anchored to the DNA phosphate backbone,
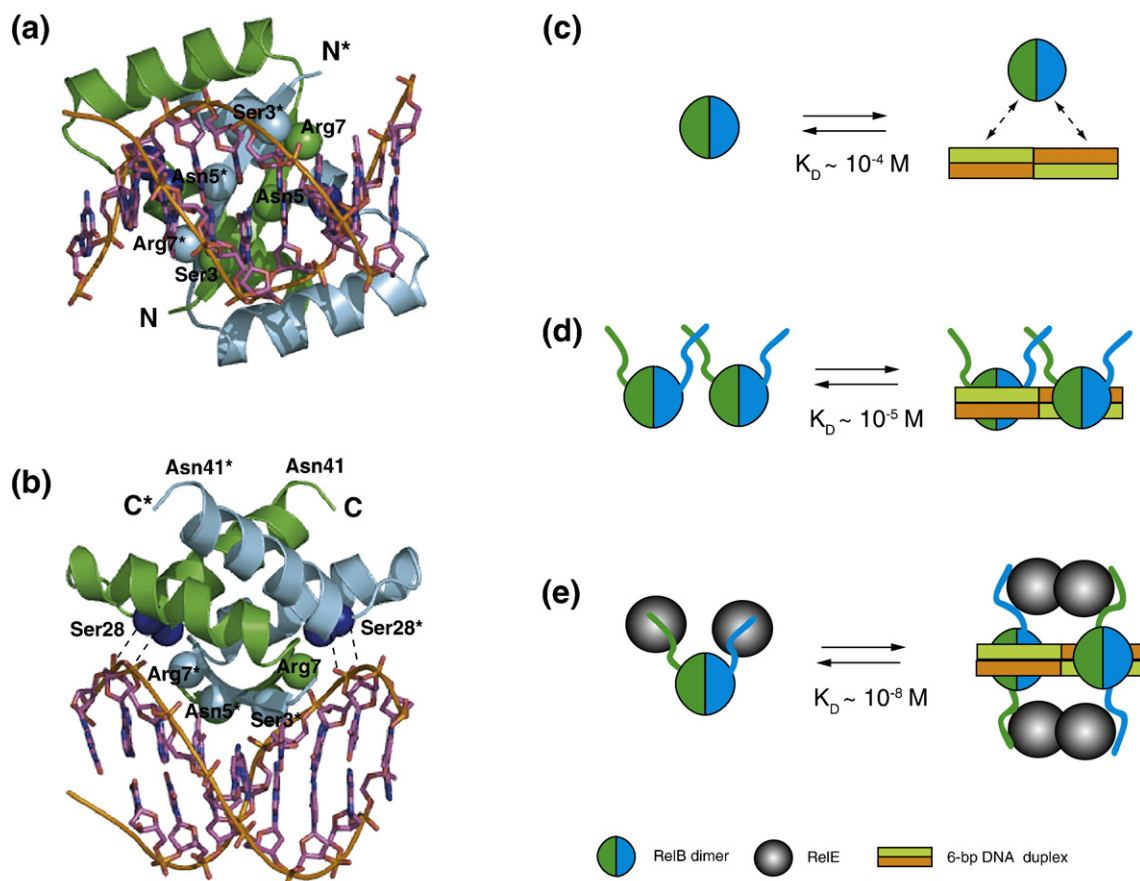
Fig. 5. A model of the RelB–DNA complex and the mechanism of autorepression of the RelBE system. (a) Homology model of RelB$_N$ based on the ARC–DNA complex (PDB code: 1BDT) bound to a 12-bp dsDNA-I fragment. (b) The side view of (a) by 90° rotation along the *x*-axis. The cartoon diagrams of (c) RelB$_N$ dimer, (d) RelB tetramer, and (e) RelB–RelE octamer bound to the operator DNA.

on either side of the major groove, by nonspecific contacts between protein backbone amide groups (Ser28 and Glu29) and DNA phosphate groups.

Discussion

Gene transcription of *relBE* TA module is negatively autoregulated by their protein products.[1,10,23,24] While previous biochemical and structural studies have focused on the antitoxin–toxin function of RelB and RelE, little is known about the structural basis of the autorepression mechanism of this TA system. Here, we have biochemically and structurally characterized the components of this system and their mutual interactions in order to shed light on the mechanisms of regulation at the molecular level.

Our CD and NMR analyses of *E. coli* RelB antitoxin indicate that RelB possesses substantial secondary structure (53% α-helical) mainly localized in a compact protease-resistant core domain at its N-terminus. By contrast, the C-terminal part of RelB is less structured and more sensitive to proteolysis. Such findings are consistent with the different thermal stabilities exhibited by RelB$_N$ (T_m, 65 °C) and RelB$_C$ (T_m, <10 °C). The N-terminal core domain

adopts the RHH transcription factor fold with a sequence-specific DNA binding activity (Fig. 5a and b), while the C-terminal domain is highly flexible and appears to undergo induced folding upon binding to toxin RelE.[14] This bipartite organization with distinct domains for DNA binding and toxin binding has been observed in several TA modules.[21,22,37,38]

One of the novel features of RelB in contrast to other antitoxins is its oligomerization property. Our SEC, MALS, and CCL analyses (Table 1) demonstrated that the full-length RelB forms a tetramer in solution. However, CcdA,[21] ParD,[22] and ParG[39] antitoxins have been reported to form a dimer under comparable conditions. We found that tetramerization of RelB involves dimerization of dimers mediated by the predicted helix in the C-terminal region (Fig. S1), since the C-terminal truncation of RelB appeared to change its oligomeric state (Table 1). RelB$_{1–79}$ and RelB$_{1–70}$ were tetrameric whereas RelB$_{1–65}$ and RelB$_{1–50}$ were dimeric. RelB$_{1–70}$ is only five residues longer than the trypsin-resistant RelB$_{1–65}$ but includes the full length of the putative helix α3. These C-terminal residues of the third helix, including Leu66, may be important to establish the amphipathic nature of the helix α3 (Fig. S1). This observation suggests that the structural integ-

rity and amphipathic nature of this helix is crucial for the dimerization of RelB dimers. The disassociation constant (K_d) of tetramerization can be estimated at an approximate range of 10^{-5} M from our *in vitro* experiments, including gel filtration chromatography and NMR spectroscopy. This weak homotetramerization of RelB may not occur at the physiological concentration of the protein. The DNA gel shift assay with RelB alone (Fig. 2c) indicated the formation of a higher-order oligomerization of RelB when it binds to the DNA promoter region with multiple binding sites. Nevertheless, the propensity of RelB to form a tetramer may help in the preorganization of the two RHH motifs for RelB–DNA interaction.

Our NMR data showed the presence of doublet peaks in the spectra of RelB tetramers $RelB_{1-79}$ and $RelB_{1-70}$ (Figs. 1c and S2a). This peak doubling was observed for a number of residues, most significantly for residues in the loop $\alpha2-\alpha3$ region (R43 and F46), which links the N- and C-terminal domains. By contrast, in the spectra of $RelB_{1-65}$ and $RelB_{1-50}$, we observed only single peaks for these residues. It is most likely that there is some asymmetry between the two dimeric subunits that comprise a tetramer. In this respect, RelB is similar to the tetrameric Mnt repressor (maintenance of lysogeny) of *Salmonella* bacteriophage P22.[40] The full-length Mnt_{1-82} forms a tetramer, but the C-terminal deletion mutant Mnt_{1-78} is a dimer. The C-terminal tetramerization domain of Mnt_{52-82} forms an unusual asymmetrical four-helix bundle.[41]

Similar to the archaeal $aRelB_2-aRelE_2$ from *P. horikoshii*,[12] the *E. coli* RelB and RelE were purified as a stable $RelB_2-RelE_2$ heterotetrameric complex (Table 1). However, unlike aRelB that interacts with aRelE toxin using a large area of the interface (Fig. S1b), the toxin-binding region of the *E. coli* RelB resides in the less folded C-terminal part, $RelB_C$ (our unpublished data and another group's data[14]). Its N-terminal domain forms a compact dimeric RHH structure through numerous hydrophobic contacts (Fig. 3). Due to the relatively small area of $RelB_C$ involved in both self-association and RelE binding, it is conceivable to speculate that the weak self-tetramerization of RelB (K_d, $>10^{-5}$ M) is disrupted by the tight RelE binding (K_d, $<10^{-7}$ M). Accordingly, the $RelB_2-RelE_2$ complex could exhibit in such a way that a RelB dimer interacts with two RelE through the C-terminal tails of each subunit (Fig. 5e). Despite the sequence and structure homology of aRelE and RelE toxins,[14] aRelB and RelB diverged to adapt structures to their "own" hosts, which may have resulted from mixing and matching of antitoxin and toxin genes.[11]

The present study has provided direct evidence that a RelB dimer recognizes the hexad repeats in its own promoter region through an RHH motif. A homology model of a $RelB_N$–DNA complex (Fig. 5a and b) shows that the $RelB_N$ dimer inserts its positively charged β-sheet into the major groove of DNA at the central position of the hexad repeat. The hydrophilic side chains of residues Ser3, Asn5, and

Arg7 determine the sequence specificity by contacting the nucleotide bases. The backbone amide groups of residues Ser28 and Glu29 from the N-terminal of the helix α2 make nonspecific anchor contacts with the DNA phosphate backbone.

In our gel mobility shift assay, we observed multiple bands corresponding to more than one RelB molecule bound to the DNA template, which demonstrates the presence of a number of subsites on the promoter region with different affinities for RelB binding (Fig. 2c). Inspection of the nucleotide sequence of the *relBE* promoter indicated that there are four central operator elements: O_{R1}, O_{R2}, and O_{L1} match a consensus sequence of 5′-TT(G/A)(T/C)AA-3′, whereas O_{L2} possesses a similar sequence of TgACAt (Fig. 2a). External to these contiguous tandem repeat elements, two additional elements with weak similarities reside at both upstream and downstream locations (TTGTAg and gTGTAA, respectively). We determined that the RelB–RelE complex binds the DNA template encoding the central operator elements with high affinity (K_d, $\sim10^{-8}$ M) in a highly cooperative manner (Table 2). This is presumably owing to the formation of a stable tetramer of RelB mediated by RelE binding to the C-terminal tail of RelB (Fig. 5e). The removal of RelE from the SPR binding assay dramatically reduced the DNA-binding activity of RelB (K_d, $\sim10^{-5}$ M). In this situation, RelB dimers recognize the 6-bp operator element but lack the cooperativity and high affinity exhibited by the RelB–RelE complex. However, as demonstrated by MALS and gel filtration experiments, RelB forms a weakly associated tetramer via the interaction between the C-terminal tails (Fig. 5d). This self-association enhances DNA binding activity (K_d, $\sim10^{-5}$ M) compared to the dimeric $RelB_N$ domain (K_d, $\sim10^{-4}$ M) (Fig. 5c). These data suggest that the transcriptional effect of RelB possesses two levels of transcriptional regulation. At high concentrations of toxin RelE, the transcription of both genes is highly suppressed by formation of the RelB–RelE complex. At low concentrations of RelE, the transcriptional repression by RelB is reduced because of the weak DNA binding activity of RelB alone. This hierarchy of transcriptional repression mechanisms provides a graded cellular response to a wide range of RelE concentration, which may be crucial to cell survival.

The functionality of RelE as a corepressor may be achieved by promoting RelB–DNA interaction through altering RelB to a conformation optimal for DNA binding or by creating a protein surface of the RelB–RelE complex that is complementary to the DNA surface. Based on our present studies and the available crystal structure of FitAB–DNA complex,[42] we have summarized our current knowledge and hypothesized on how RelE enhances the RelB–DNA complex (Fig. 5e). Since the RelB self-tetramerization region overlaps with the RelE-binding region at the C-terminal of RelB, we speculate that RelE disrupts the weak self-association of RelB (Fig. 5d) by recognizing the C-terminal tail with a specific and tight interaction (Fig. 5e). Two RelE molecules can be

bundled together by the tails of two RelB molecules as seen in the structure of the aRelB–aRelE complex.[12] In this organization, a pair of RHH dimeric domains of RelB binds to the adjacent binding sites on DNA promoter region (Fig. 5e). The resultant RelB$_4$–RelE$_4$ complex may form a tight association with two adjacent binding sites on the promoter, which could involve either DNA bending or DNA-induced protein conformational change. Such synergistic protein–protein and protein–DNA interactions may provide a molecular basis for the high-affinity binding between the transcriptional repressor–corepressor complex and the promoter DNA.

Methods and Experiments

Protein expression and purification

RelB and its mutants (1–70, 1–65, 1–50, and R7A) were expressed as His tag fusion proteins from the pET28a plasmid. RelB$_{C(47–79)}$ peptide was expressed as a glutathione *S*-transferase fusion protein from the pGEX2T plasmid. The RelB–RelE protein complex was coexpressed from the *relBE* operon with the pET expression system, which enabled us to express the two cognate genes under the same promoter. In order to copurify the RelB–RelE complex, two expression vectors were constructed: pET28a and pET21cc. The former system encodes a cleavable N-terminal His-tagged RelB (upstream) and an untagged RelE (downstream), and the later plasmid encodes untagged RelB and a C-terminal His-tagged RelE without any cleavage site. All proteins were expressed in the *E. coli* strain of BL21(DE3). The cells were grown in LB or M9 media at 37 °C and induced by 1 mM IPTG for 10–12 h at 23 °C. RelB proteins and RelB–RelE complexes were purified by affinity (Ni-NTA and glutathione Sepharose for His tag and glutathione *S*-transferase fusion protein, respectively) and gel filtration chromatography. All cleavable fusion tags were removed after affinity column by thrombin digestion.

CD spectroscopy

All protein samples are prepared in 20 mM sodium phosphate buffer, pH 7.0, and 50 mM NaCl at a monomer concentration of 20 μM. CD spectra were performed in a Jasco J-810 spectropolarimeter at a scan rate of 20 nm/min and 8 s response with a 0.5-nm data pitch, using 1 nm bandwidth for two accumulations at 20 °C. Temperature scans were performed at 222 nm, with a temperature change rate of 1.5 °C/min and 2 s response from 5 to 95 °C.

SEC and MALS

SEC was performed on Superdex 75 10/30 or 26/60 GL columns using AKTA FPLC system (GE Healthcare Life Sciences) at 4 °C in a buffer of 20 mM NaPi, pH 7.0, 100 mM NaCl, and 1 mM DTT. MALS measurements were done in-line with SEC using a three-angle (45°, 90°, and 135°) miniDawn light-scattering photometer equipped with a 690-nm laser and an Optilab rEX differential refractometer (Wyatt Technologies, Inc.). Molecular weight was calculated using the ASTRA software (Wyatt Technologies, Inc.) based on Zimm plot analysis and using a protein refractive index increment (*dn/dc*) at 0.185 l/g.

In vitro transcription assay of *relBE* gene

A *relBE* DNA fragment covering the *relBE* promoter region (5 pmol aliquot) was preincubated with 0.5 μg *E. coil* RNA polymerase in transcription buffer (40 mM Tris–Cl, pH 7.5, 10 mM MgCl$_2$, and 100 mM KCl) at 37 °C for 15 min. Differing amounts of the RelB–RelE complex or RelB were then added together with 10 μCi of [α-^{32}P]-CTP, 1.2 mM ApC, and NTP mixture. The reaction took place at 37 °C for 20 min. As a control, a *mazG* mRNA fragment was incubated in the transcription buffer at 37 °C for 20 min and mixed with the RelB–RelE complex or RelB. Reaction products were analyzed by 6% polyacrylamide–urea gel followed by autoradiography.

Electrophoretic mobility shift assay (EMSA)

A 150-bp *relBE* DNA fragment covering the *relBE* promoter region and the first 57 bp downstream of the *relBE* translational start was amplified by PCR and end labeled using Klenow DNA polymerase. The RelB–RelE complex or RelB was mixed at different concentrations with 2 μl of the end-labeled DNA fragment in buffer A containing 200 mg/l poly(dI–dT) [50 mM Tris–Cl (pH 7.5), 5 mM MgCl$_2$, 5% glycerol, and 1 mM DTT] at room temperature for 15 min. Reaction products were analyzed by 10% native polyacrylamide gel electrophoresis followed by autoradiography.

DNase I footprinting assay

Differing amounts of RelB–RelE and RelB were mixed with 2 μl of the DNA fragment used in EMSA in buffer A [50 mM Tris–Cl (pH 7.5), 5 mM MgCl$_2$, 5% glycerol, and 1 mM DTT] containing 200 mg/l poly(dI–dT) at room temperature for 15 min. DNase I (0.25 U; Promega) was added to the resultant mixtures and then mixed at room temperature for 2 min. The reaction was stopped by 12 μl of the loading buffer (95% formamide, 20 mM ethylenediaminetetraacetic acid, 0.05% bromophenol blue, and 0.05% xylene cyanol EF). The sample was incubated at 90 °C for 5 min prior to electrophoresis on 8% polyacrylamide sequencing gel followed by autoradiography.

Surface plasmon resonance

SPR experiments were performed using a BIAcore 2000 instrument (Biacore AB). Three DNA fragments including the different lengths of the operator sequences (dsDNA-I, 12 bp with one repeat equivalent to a half site of O$_L$ or O$_R$; dsDNA-II, 20 bp with two repeats, equivalent to the O$_R$; dsDNA-III, 32-bp with four repeats, O$_L$ + O$_R$) were synthesized with the top strands modified with a 5′-biotinyl-TEG motif. Annealed dsDNA-I, -II, and -III fragments were immobilized to flow cells 2, 3, and 4 of a streptavidin-coated sensor chip at approximately 1000 RU, respectively. Flow cell 1 was blocked with biotin and served as the reference channel.

RelB proteins and the RelB–RelE complex in the SPR running buffer (20 mM NaPi, pH 7.0, 50 mM NaCl, 5 mM MgCl$_2$, 0.1 mM DTT, 0.2 mg/ml bovine serum albumin,

and 0.002% P20 surfactant) were injected for 2 min at a flow rate of 25 μl/min. After measuring the off rates for 2 min for each analyte injection, regeneration of the surface was achieved with a 1-min injection of 2 M NaCl. For RelB proteins, the steady-state affinity was determined from curve fitting to a plot of the R_{eq} values, derived from sensorgrams fitted locally, against the concentrations. The apparent affinities of the RelB–RelE complex were determined by globally fitting with the kinetic simultaneous k_a/k_d model, assuming one-site Langmuir (1:1) binding or two-site heterogeneous ligand.

NMR spectroscopy

NMR samples were prepared in 20 mM NaPi, pH 6.5, 100 mM NaCl, 1 mM DTT, 1 mM NaN$_3$, and 10% D$_2$O, at concentrations of 0.8–1.0 mM for triple-resonance and NOESY experiments and 0.3 mM for DNA titrations. The DNA fragments (dsDNA-I or -II) were incrementally added from 0 to 0.6 mM. NMR data were collected at 30 °C on Varian Unity/INOVA 500, 600 MHz and AVANCE II Bruker 800 MHz, all equipped with a triple-resonance z-gradient cryoprobe probe. The NOE connectivity was assigned with 3D ^{15}N-edited NOESY and 3D ^{13}C-edited NOESY spectra. The intermolecular NOE was detected with a 3D ^{15}N/^{13}C-edited (t_1) and ^{15}N/^{13}C-filtered (t_2) NOESY–HSQC experiment[27] on a mixture of 50% ^{15}N,^{13}C-labeled and 50% unlabeled samples. All spectra were processed with NMRPipe and analyzed using the programs NMRView[43] and XEASY.[44]

Structure calculation and refinement

The NMR solution structures were generated using the CYANA.[28] Automatic calibration was used to convert the NOE peak intensities into distance constraints. Unambiguous assignments of intermolecular NOEs from the ^{15}N/^{13}C-edited (t_1) and ^{15}N/^{13}C-filtered (t_2) NOESY–HSQC spectrum were determined manually. The 48 intermolecular distances together with 34 dihedral angles calculated from chemical shift using TALOS[45] and 26 hydrogen bonds for regions of regular β-strand or α-helix derived from CSI analysis were kept during the calculations. The final structure of RelB$_N$ was refined using CNS[29] with NH dipolar coupling restraints as input and water as the explicit solvent. The structures were analyzed using PROCHECK–NMR.[46]

Modeling of RelB$_N$–DNA complex

Homology models of RelB$_N$ complexed with DNA were built using structures of Arc/DNA [Protein Data Bank (PDB) code: 1BDT][36] and ω/DNA (PDB code: 2BNZ)[26] as templates. For each template, a RelB$_N$ dimer was superimposed onto the template RHH dimer structure by fitting the backbone of RelB$_N$ β-strand residues 3–7 (both subunits) to the equivalent residues (residues 9–13 of Arc, 27–31 of ω) using PyMOL.[35] The nucleotide sequence of the template DNA was mutated into *relBE* operator sequence with COOT.[47] The resultant models were refined by energy minimization using CNS[40] to remove steric clashes.

Database deposition information

NMR data as well as atomic coordinates and structure factors have been deposited in the Biological Magnetic Resonance Bank with accession code 15691 and in the PDB with accession code 2k29.

Supplementary Data

Supplementary data associated with this article can be found, in the online version, at doi:10.1016/j.jmb.2008.04.039

References

1. Engelberg-Kulka, H. & Glaser, G. (1999). Addiction modules and programmed cell death and antideath in bacterial cultures. *Annu. Rev. Microbiol.* **53**, 43–70.
2. Hayes, F. (2003). Toxins–antitoxins: plasmid maintenance, programmed cell death, and cell cycle arrest. *Science,* **301**, 1496–1499.
3. Gerdes, K., Christensen, S. K. & Lobner-Olesen, A. (2005). Prokaryotic toxin–antitoxin stress response loci. *Nat. Rev., Microbiol.* **3**, 371–382.
4. Sevin, E. W. & Barloy-Hubler, F. (2007). RASTA-Bacteria: a web-based tool for identifying toxin–antitoxin loci in prokaryotes. *Genome Biol.* **8**, R155.
5. Jensen, R. B. & Gerdes, K. (1995). Programmed cell death in bacteria: proteic plasmid stabilization systems. *Mol. Microbiol.* **17**, 205–210.
6. Pandey, D. P. & Gerdes, K. (2005). Toxin–antitoxin loci are highly abundant in free-living but lost from host-associated prokaryotes. *Nucleic Acids Res.* **33**, 966–976.
7. Christensen, S. K., Mikkelsen, M., Pedersen, K. & Gerdes, K. (2001). RelE, a global inhibitor of translation, is activated during nutritional stress. *Proc. Natl Acad. Sci. USA,* **98**, 14328–14333.
8. Christensen, S. K. & Gerdes, K. (2003). RelE toxins from bacteria and Archaea cleave mRNAs on translating ribosomes, which are rescued by tmRNA. *Mol. Microbiol.* **48**, 1389–1400.
9. Pedersen, K., Zavialov, A. V., Pavlov, M. Y., Elf, J., Gerdes, K. & Ehrenberg, M. (2003). The bacterial toxin RelE displays codon-specific cleavage of mRNAs in the ribosomal A site. *Cell,* **112**, 131–140.
10. Gronlund, H. & Gerdes, K. (1999). Toxin–antitoxin systems homologous with relBE of *Escherichia coli* plasmid P307 are ubiquitous in prokaryotes. *J. Mol. Biol.* **285**, 1401–1415.
11. Anantharaman, V. & Aravind, L. (2003). New connections in the prokaryotic toxin–antitoxin network: relationship with the eukaryotic nonsense-mediated RNA decay system. *Genome Biol.* **4**, R81.
12. Takagi, H., Kakuta, Y., Okada, T., Yao, M., Tanaka, I. & Kimura, M. (2005). Crystal structure of archaeal toxin–antitoxin RelE–RelB complex with implications for

toxin activity and antitoxin effects. *Nat. Struct. Mol. Biol.* **12**, 327–331.

13. Buts, L., Lah, J., Dao-Thi, M. H., Wyns, L. & Loris, R. (2005). Toxin–antitoxin modules as bacterial metabolic stress managers. *Trends Biochem. Sci.* **30**, 672–679.

14. Cherny, I., Overgaard, M., Borch, J., Bram, Y., Gerdes, K. & Gazit, E. (2007). Structural and thermodynamic characterization of the *Escherichia coli* RelBE toxin–antitoxin system: indication for a functional role of differential stability. *Biochemistry*, **46**, 12152–12163.

15. Johnson, W. C. (1999). Analyzing protein circular dichroism spectra for accurate secondary structures. *Proteins: Struct. Funct. Genet.* **35**, 307–312.

16. Jones, D. T. (1999). Protein secondary structure prediction based on position-specific scoring matrices. *J. Mol. Biol.* **292**, 195–202.

17. Wang, A. C., Lodi, P. J., Qin, J., Vuister, G. W., Gronenborn, A. M. & Clore, G. M. (1994). An efficient triple-resonance experiment for proton-directed sequential backbone assignment of medium-sized proteins. *J. Magn. Reson., Ser. B*, **105**, 196–198.

18. Grzesiek, S. & Bax, A. (1993). Amino acid type determination in the sequential assignment procedure of uniformly $^{13}C/^{15}N$-enriched proteins. *J. Biomol. NMR*, **3**, 185–204.

19. Wishart, D. S. & Sykes, B. D. (1994). The ^{13}C chemical-shift index: a simple method for the identification of protein secondary structure using ^{13}C chemical-shift data. *J. Biomol. NMR*, **4**, 171–180.

20. Loris, R., Marianovsky, I., Lah, J., Laeremans, T., Engelberg-Kulka, H., Glaser, G. *et al.* (2003). Crystal structure of the intrinsically flexible addiction antidote MazE. *J. Biol. Chem.* **278**, 28252–28257.

21. Madl, T., Van Melderen, L., Mine, N., Respondek, M., Oberer, M., Keller, W. *et al.* (2006). Structural basis for nucleic acid and toxin recognition of the bacterial antitoxin CcdA. *J. Mol. Biol.* **364**, 170–185.

22. Oberer, M., Zangger, K., Gruber, K. & Keller, W. (2007). The solution structure of ParD, the antidote of the ParDE toxin–antitoxin module, provides the structural basis for DNA and toxin binding. *Protein Sci.* **16**, 1676–1688.

23. Bech, F. W., Jorgensen, S. T., Diderichsen, B. & Karlstrom, O. H. (1985). Sequence of the relB transcription unit from *Escherichia coli* and identification of the relB gene. *EMBO J.* **4**, 1059–1066.

24. Gotfredsen, M. & Gerdes, K. (1998). The *Escherichia coli* relBE genes belong to a new toxin–antitoxin gene family. *Mol. Microbiol.* **29**, 1065–1076.

25. Dao-Thi, M. H., Charlier, D., Loris, R., Maes, D., Messens, J., Wyns, L. & Backmann, J. (2002). Intricate interactions within the ccd plasmid addiction system. *J. Biol. Chem.* **277**, 3733–3742.

26. Weihofen, W. A., Cicek, A., Pratto, F., Alonso, J. C. & Saenger, W. (2006). Structures of omega repressors bound to direct and inverted DNA repeats explain modulation of transcription. *Nucleic Acids Res.* **34**, 1450–1458.

27. Konrat, R., Muhandiram, D. R., Farrow, N. A. & Kay, L. E. (1997). Pulse schemes for the measurement of 3JC ′C gamma and 3JNC gamma scalar couplings in $^{15}N,^{13}C$ uniformly labeled proteins. *J. Biomol. NMR*, **9**, 409–422.

28. Guntert, P., Mumenthaler, C. & Wuthrich, K. (1997). Torsion angle dynamics for NMR structure calculation with the new program DYANA. *J. Mol. Biol.* **273**, 283–298.

29. Brunger, A. T., Adams, P. D., Clore, G. M., DeLano, W. L., Gros, P., Grosse-Kunstleve, R. W. *et al.* (1998). Crystallography and NMR system: a new software suite for macromolecular structure determination. *Acta Crystallogr., Sect. D: Biol. Crystallogr.* **54**, 905–921.

30. Breg, J. N., van Opheusden, J. H., Burgering, M. J., Boelens, R. & Kaptein, R. (1990). Structure of Arc repressor in solution: evidence for a family of beta-sheet DNA-binding proteins. *Nature*, **346**, 586–589.

31. Somers, W. S. & Phillips, S. E. (1992). Crystal structure of the met repressor–operator complex at 2.8 Å resolution reveals DNA recognition by beta-strands. *Nature*, **359**, 387–393.

32. Schreiter, E. R. & Drennan, C. L. (2007). Ribbon–helix–helix transcription factors: variations on a theme. *Nat. Rev., Microbiol.* **5**, 710–720.

33. Wilson, D. N. & Nierhaus, K. H. (2005). RelBE or not to be. *Nat. Struct. Mol. Biol.* **12**, 282–284.

34. Baker, N. A., Sept, D., Joseph, S., Holst, M. J. & McCammon, J. A. (2001). Electrostatics of nanosystems: application to microtubules and the ribosome. *Proc. Natl. Acad. Sci. USA*, **98**, 10037–10041.

35. DeLano, W. L. (2002). *The PyMOL molecular graphics system.* DeLANO Scientific, Palo Alto, CA, USA. website at http://www.pymol.org.

36. Schildbach, J. F., Karzai, A. W., Raumann, B. E. & Sauer, R. T. (1999). Origins of DNA-binding specificity: role of protein contacts with the DNA backbone. *Proc. Natl Acad. Sci. USA*, **96**, 811–817.

37. Kamada, K. & Hanaoka, F. (2005). Conformational change in the catalytic site of the ribonuclease YoeB toxin by YefM antitoxin. *Mol. Cell*, **19**, 497–509.

38. Kamada, K., Hanaoka, F. & Burley, S. K. (2003). Crystal structure of the MazE/MazF complex: molecular bases of antidote–toxin recognition. *Mol. Cell*, **11**, 875–884.

39. Golovanov, A. P., Barilla, D., Golovanova, M., Hayes, F. & Lian, L. Y. (2003). ParG, a protein required for active partition of bacterial plasmids, has a dimeric ribbon–helix–helix structure. *Mol. Microbiol.* **50**, 1141–1153.

40. Burgering, M. J., Boelens, R., Gilbert, D. E., Breg, J. N., Knight, K. L., Sauer, R. T. & Kaptein, R. (1994). Solution structure of dimeric Mnt repressor (1–76). *Biochemistry*, **33**, 15036–15045.

41. Nooren, I. M., Kaptein, R., Sauer, R. T. & Boelens, R. (1999). The tetramerization domain of the Mnt repressor consists of two right-handed coiled coils. *Nat. Struct. Biol.* **6**, 755–759.

42. Mattison, K., Wilbur, J. S., So, M. & Brennan, R. G. (2006). Structure of FitAB from *Neisseria gonorrhoeae* bound to DNA reveals a tetramer of toxin–antitoxin heterodimers containing pin domains and ribbon–helix–helix motifs. *J. Biol. Chem.* **281**, 37942–37951.

43. Johnson, B. A. (2004). Using NMRView to visualize and analyze the NMR spectra of macromolecules. *Methods Mol. Biol.* **278**, 313–352.

44. Bartels, C., Xia, T., Billeter, M., Guntert, P. & Wuthrich, K. (1995). The program XEASY for computer-supported NMR spectral analysis of biological macromolecules. *J. Biomol. NMR*, **6**, 1–10.

45. Cornilescu, G., Delaglio, F. & Bax, A. (1999). Protein backbone angle restraints from searching a database for chemical shift and sequence homology. *J. Biomol. NMR*, **13**, 289–302.

46. Laskowski, R. A., Rullmannn, J. A., MacArthur, M. W., Kaptein, R. & Thornton, J. M. (1996). AQUA and PROCHECK–NMR: programs for checking the quality of protein structures solved by NMR. *J. Biomol. NMR*, **8**, 477–486.

47. Emsley, P. & Cowtan, K. (2004). Coot: model-building tools for molecular graphics. *Acta Crystallogr., Sect. D: Biol. Crystallogr.* **60**, 2126–2132.